Journal of Nanoparticle Research: An Interdisciplinary Forum for Nanoscale Science and Technology© Springer Science+Business Media Dordrecht 2013. 10.1007/s11051-013-2140-1

Research Paper

Synergetic effect of CdS quantum dots and TiO_2 nanofibers for photoelectrochemical hydrogen generation

S. Chaguetmi[1, 2, 3], F. Mammeri[1], M. Pasut[1], S. Nowak[1], H. Lecoq[1], P. Decorse[1], C. Costentin[4],S. Achour[3] and S. Ammar[1]

(1) Interfaces, Traitements, Organisation et Dynamique des Systèmes, Université Paris Diderot, CNRS UMR7086, Sorbonne Paris Cité, 15 rue Jean-Antoine de Baïf, Paris Cedex 13, France
(2) Université 20 Août 1955 de Skikda, Skikda, Algeria
(3) Laboratoire de Céramique, Université de Constantine 1, Constantine, Algeria
(4) Laboratoire d'Electrochimie Moléculaire, Université Paris Diderot, CNRS UMR7591, Sorbonne Paris Cité, Paris, France

S. Ammar
Email: ammarmer@univ-paris-diderot.fr

Received: 24 July 2013**Accepted:** 18 November 2013**Published online:** 30 November 2013

Abstract

In this work, we developed a new type of nanostructured photoanodes for photoelectrochemical water splitting. They are based on CdS–TiO_2 nanocomposite films, supported on conductive Ti sheets, prepared by an easy-to-achieve three-step method. It involves the production of TiO_2 nanofibers (NFs) using a controlled corrosion route of polished Ti sheets, the preparation of size-controlled CdS quantum dots (QDs) by the polyol process and the direct impregnation of TiO_2/Ti sheets by QDs in suspension. The photoelectrochemical (PEC) properties of the resulting nanostructures were measured, using a homemade electrochemical cell illuminated with a standard Xenon lamp, and compared to those of bare TiO_2 NFs. A net enhancement of the photocurrent was observed after CdS impregnation, suggesting a low carrier recombination rate and a higher efficiency of the PEC device for solar water splitting, as the induced photocurrent is related to the electrons needed to reduce H^+ ions into H_2 at the cathode electrode (Pt wire).

Keywords

TiO_2 nanofibers CdS quantum dots CdS–TiO_2/Ti nanocomposites Photoelectrochemical properties X-ray photoelectron spectroscopy Electron microscopy Energy conversion

Introduction

Hydrogen generation from solar light-driven water splitting using efficient photoelectrochemical cells (PECs) with advanced photoelectrodes is one of the most exciting issues in the R&D Departments in materials for energy (Lewis and Nocera *2006*). Nowadays, this technology is assumed to be the most promising one for hydrogen production since PEC technology is based on sustainable solar energy and abundant water resources. Moreover, it is environmentally safe, with no undesirable by-products. It may be used on both small and large scales since it is relatively easy to achieve (Bak et al. *2002*).

The development of efficient photoanodes is still in progress since their property requirements, in terms of semiconducting and electrochemical properties and their impact on the performance of PECs, have to be improved in order to reach an efficient charge separation in the photoelectrodes and charge transfer within PECs, under the lowest possible PEC voltage for water decomposition. For water photodecomposition to occur, the potential of the top of the valence band has to be more positive with respect to the oxidation potential of the reaction $2OH^- + 2h^+ \rightarrow H_2O + ½O_2$ and the potential corresponding to the bottom of the conduction band has to be more negative with respect to the reduction potential of the reaction ($2H^+ + 2e^- \rightarrow H_2$). This means that the band edges of the electrode must overlap with the acceptor and donor states of water decomposition reaction, thus requiring that the electrode should at least exhibit a bandgap of 1.23 eV, in such a way to promote both the oxidation and reduction simultaneously. In addition, the charge transfer from the surface of the semiconductor must be fast enough to prevent photocorrosion. Nanocrystalline mesoporous semiconductor materials can achieve considerable conversion efficiency because of their high internal surface area and small local electric field as well as the flexibility of their bandgap tailoring.

Several materials were considered to process such photoelectrodes; among them, nanostructured titania, particularly in its 1D shape (nanofibers, nanotubes, or nanorods…), has attracted much attention. Due to its unique chemical, electrical, and light-dependent properties, a lot of studies were carried out in order to integrate it in various light-harvesting devices. Indeed, the cheap fabrication, chemical stability, high specific surface area, photosensitivity, and catalytic potential of TiO_2 nanostructures make them valuable as photocatalytic and photoelectrocatalytic supports (Cao et al.*2012*; Mor et al. *2005*; John et al. *2009*; Allam and Grimes *2009*; Xie *2006*; Pokhrel et al. *2008*; Tian et al. *2010*; Kawahara et al. *2002*; Kasuga et al. *1999*; Lin et al. *2009*). Unfortunately, they suffer from low optical quantum efficiency. Indeed, because of its relatively wide semiconducting gap, TiO_2 usually only harvest the UV light which represent only 5 % of sunlight, resulting in low energy conversion efficiency. To overcome this drawback and increase TiO_2 visible light absorption, doping (Asahi et al.*2001*), or sensitization with small bandgap semiconductors (Vogel et al. *1994*; Banerjee et al. *2008*; Shen et al. *2006*; Seabold et al. *2008*; Gao et al. *2009*) or combination of doping and sensitization (Hensel et al. *2010*) are nowadays seriously investigated.

Focusing on sensitization approach, combining TiO_2 with narrow bandgaps II–VI nanocrystals, such as CdS, CdSe, or CdTe [called here quantum dots (QDs)], appears

particularly promising. Indeed, such QD nanocrystals exhibit (i) exceptional photo absorption properties which can be tuned from IR to UV ranges by varying their average size, (ii) an excellent photostability, and (iii) a high quantum yield (Louie*2010*). Nowadays, a rich literature describes the preparation of such QD-TiO_2 hetero-nanostructures, using different material processing routes, and reports their PEC properties in various experimental conditions. For instance, producing and depositing simultaneously the QDs on TiO_2 nanostructures was explored through different routes such as electrochemical deposition (Chen et al. *2006*; Wang et al. *2009*; Yin et al.*2007*), sequential-chemical bath deposition (S-CBD) (Sun et al. *2008*; Baker and Kamat *2009*; Lin et al. *2009*; Zhang et al. *2009*), and successive ion-layer adsorption and reaction method (Zhang et al. *2010*). In almost all these cases, TiO_2nanostructures were fully coated by QDs as a continuous layer or as a percolated network. Moreover, PEC properties appeared to be dependent not only on the nature of QDs but also on the synthesis and deposition conditions, making hydrogen generation particularly sensitive to the photoelectrode processing method. Surprisingly, methods based on a subsequent QD grafting on preformed TiO_2nanostructures were seldom described, even if they allow (i) an efficient control of the morphology and thus of the optical properties of the grafted semiconductors, (ii) an optimization of the minimal QDs amount (due to their intrinsic toxicity) in the final architecture to lead to the best PEC results, and (iii) an improvement of TiO_2processing as less structure and microstructure perturbing.

Hence, on the basis of this knowledge, we aim at (i) producing size calibrated (2 nm) and highly crystallized CdS QDs using the well-known polyol process (Gaceur et al.*2012*; Feldman and Metzmacher *2001*); (ii) producing high surface area TiO_2nanofibers (NFs) by a non-conventional route, namely hydrothermal corrosion of Ti sheets (Wu et al. *2009*), allowing both photosensitivity (TiO_2 part) and conductivity (Ti part) which are essential for the conception of efficient photoanodes; (iii) depositing, by impregnation, a few amount of polyol-made CdS QDs on these TiO_2 NFs; and (iv) investigating the synergetic properties of the resulting CdS–TiO_2/Ti nanocomposite films toward water photoelectrolysis and hydrogen generation using a homemade PEC cell.

Experimental sections

Sample preparation

Synthesis of TiO_2 NFs supported on Ti sheets

TiO_2 NFs supported on Ti sheets were produced by controlled hydrothermal corrosion of Ti (Wu et al. *2009*). Typically, Ti sheets (0.5 mm thick, area equal to 2×1 cm^2) were chemically polished, treated by sonication in ethanol, and pickled in a 5 wt% of oxalic acid aqueous solution at 100 °C for 2 h, followed by rinsing with deionised water and drying. The pre-treated Ti sheets were immersed in a solution of 5 mL of H_2O_2(30 wt%) and 5 mL of NaOH (10 M), into a Teflon-lined stainless steel autoclave. The autoclave was heated at 80 °C for 24 h and then cooled to room

temperature (RT). The treated Ti plates were rinsed with deionised water and dried. A protonation was conducted through two cycles of ion exchange in 50 mL of HCl (0.1 M) for 2 h and followed by rinsing with deionised water and drying at 80 °C for 1 h. Finally, all samples, quoted TiO_2 and Ti, were calcinated at 400 °C for 1 h.

Synthesis of CdS colloids

CdS QDs were synthesized using the polyol process (Gaceur et al. *2012*). Typically, 0.1 mmol of cadmium acetate, 0.12 mmol of thiourea, and 0.1 mmol of trioctylphosphine oxide (TOPO) were dissolved in 80 mL of diethyleneglycol (DEG) under mechanical stirring in a four-necked flask, and heated at 180 °C (6 °C min^{-1}). The temperature was maintained for 30 min at 180 °C and cooled quickly at room temperature (RT) using an ice bath.

Synthesis of CdS–TiO_2/Ti nanocomposite films

CdS–TiO_2/Ti nanocomposite films were prepared by impregnation of CdS QDs on the surface of TiO_2 NFs. Typically, 1 mL of the as-produced CdS polyol solution was diluted in 5 mL of DEG and sonicated for 30 min at RT. Then, TiO_2/Ti sheets were immersed into the resulting solution overnight. Finally, the samples were washed three times in ethanol under sonication and dried in air.

Sample characterization

Characterization of CdS colloids

The morphology of the produced CdS QDs was studied by transmission electron microscopy (TEM) using a JEOL 2100F microscope operating at 200 kV. A drop of the polyol colloid was deposited on a carbon grid for TEM observation. The particle size was obtained from the recorded TEM images using a digital camera and SAISAM software (Microvision Instruments), calculating the surface-average particle diameter through a statistical analysis performed by counting about 200 particles considered to be spherical.

The UV–Vis absorption spectrum of the polyol-made colloids was recorded on a CARY 56^E spectrophotometer in a transmission mode.

Characterization of TiO_2/Ti and CdS–TiO_2/Ti films

The structures of the produced TiO_2/Ti substrates and their related nanocomposites were characterized by X-ray diffraction (XRD) using a Panalytical Empyrean, equipped with a multichannel detector (PIXcel 3D) and a Cu Kα X-ray source (1.5418 Å). The XRD patterns were recorded in the w-2θ Bragg–Brentano configuration using incident grazing beam (w = 1°) with a divergence slit of 1/16°. The films were fixed on a motorized sampling platform which permits to obtain a perfectly plane position. The microstructure was analyzed using a Supra40 ZEISS field emission gun scanning electron microscope (FEG-SEM) operating at 2.5 kV.

The morphology of NFs was studied by transmission electron microscopy (TEM) using a Jeol JEM-100CX-II microscope operating at 100 kV. The UV–Vis diffuse

reflectance spectra of pristine TiO_2/Ti and CdS–TiO_2/Ti nanostructures were recorded on a Perkin Elmer-Lambda 1050 spectrophotometer equipped with a PTFE-coated integration sphere.

X-ray photoelectron spectroscopy (XPS) measurements were performed on both nanostructures using a Thermo VG ESCALAB 250 instrument equipped with a micro-focused, monochromatic Al Kα X-ray source (1,486.6 eV) and a magnetic lens. The X-ray spot size was 500 μm (15 kV, 150 W). The spectra were acquired in the constant analyzer energy mode with pass energy of 150 and 40 eV for the general survey and the narrow scans, respectively. The samples were fixed on sample holders and outgassed in the fast entry airlock (2×10^{-7} mbar). The "Avantage" software was used for data acquisition and processing. The C 1s line of 285 eV was used as a reference to correct the binding energies for charge correction.

Photoelectrochemical measurements

The photoresponse of both thin film photoelectrodes (TiO_2/Ti and CdS–TiO_2/Ti) was evaluated by measuring the photocurrent density J_p, using a scanning potentiostat (Metrohm AUTOLAB PGSTAT12 Instrument). The measurement of the photocurrent density as a function of the applied potential E was performed in a standard three-electrode configuration single-compartment homemade cell, with the as-prepared samples as working electrode (WE) and Pt wire as the counter electrode (CE) (Fig. 1). The potential of the working electrode was measured using saturated calomel electrode (SCE) as a reference electrode. A solution of Na_2SO_4 (0.5 M, pH = 7) was used as an electrolyte. The device was purged with argon to remove any dissolved oxygen prior to all experiments. The photoelectrodes (0.7×1.0 cm^2) were illuminated using a 150 W Xenon lamp (ORIEL instruments).

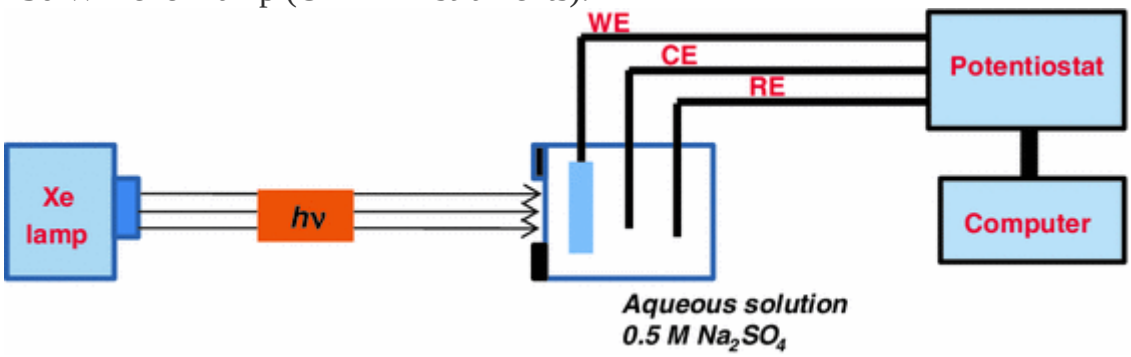

Fig. 1
Scheme of the homemade PEC cell in which CE, WE, and RE correspond to the counter electrode (Pt), working electrode (CdS–TiO_2/Ti), and the reference electrode (SCE), respectively

Results and discussion

CdS colloid characteristics

The morphology of the produced CdS nanoparticles was analyzed using TEM microscopy. The micrographs recorded on a drop of CdS polyol-based colloid

evidenced non-aggregated and almost monodisperse single crystals of about 2 nm in size (Fig. 2). The particles appear to be of high crystalline quality since they show well-defined fringes corresponding to crystallographic planes of the wurtzite lattice, with no evidence of structural defects.

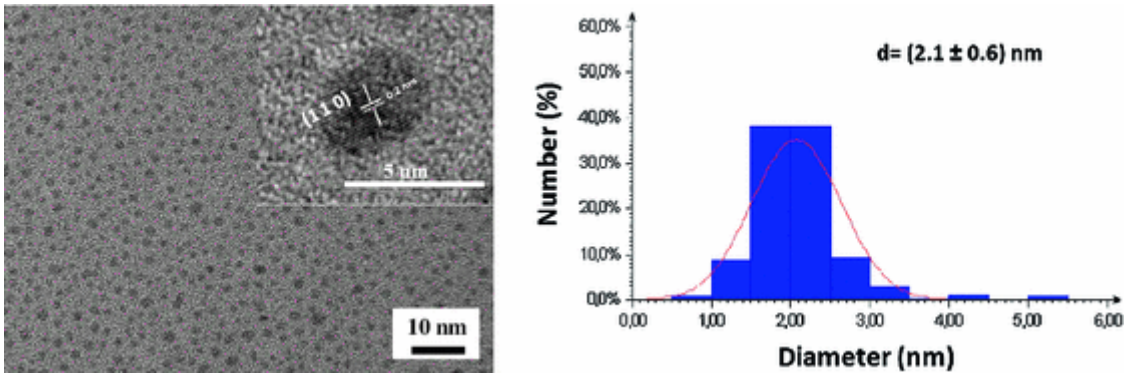

Fig. 2
TEM image of CdS QDs produced in polyol and histogram of their size distribution. HRTEM image of one representative particle is given in the *inset* and evidences an interplanar distance of 2.0 Å corresponding to the (110) planes of the wurtzite structure

The bandgap value of these semiconductors was inferred from their UV–Vis absorption spectrum recorded in a transmission mode (Fig. 3). It is evaluated to about 2.9 eV, significantly higher than that of bulk CdS (2.4 eV). This large value is due to the quantum confinement effect related to the ultrafine crystal size of the studied particles and their relative non-aggregation. The shoulder appearing at low energy may be attributed to partial absorption resulting from transitions involving surface defect levels inside the CdS bandgap and induced by particle surface oxidation. QDs surface oxidation was inferred from XPS analysis as evidenced hereafter.

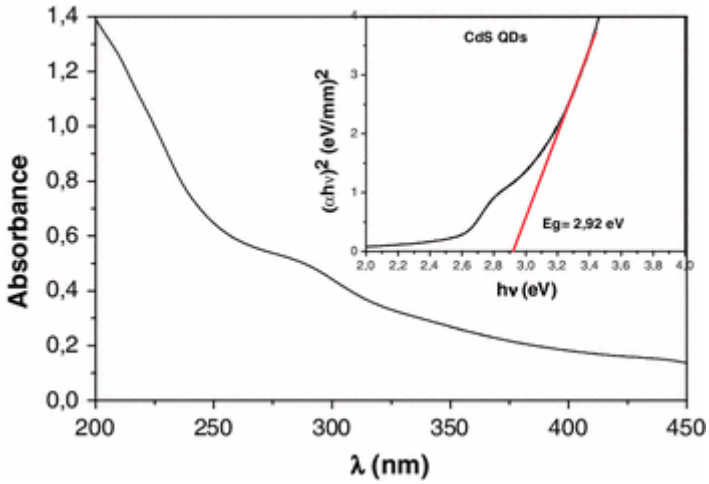

Fig. 3
Optical absorption spectrum of the polyol-based CdS colloid. The *inset* depicts the Tauc plot used to determine the bandgap value of the considered semiconductor, where *hv* is the photon energy and α is the absorption coefficient. It corresponds to the intersection between the straight portion of the curve $(\alpha hv)^2$ versus *hv* and the baseline (Liji-Sobhana et al. *2011*)

CdS–TiO_2/Ti nanocomposite film properties

Before impregnation, the corroded Ti sheets were analyzed by XRD. The recorded pattern presented in Fig. 4 exhibits 2 main peaks at 25.6° and 48.7° assigned to TiO_2anatase phase and other stronger peaks attributed to the metallic Ti substrate. Note that the peaks corresponding to the anatase phase are broadened compared to those of Ti metal, suggesting the formation of smaller in size TiO_2 anatase crystals during the corrosion treatment of larger in size metal phase (Wu et al. *2009*). After impregnation, the XRD patterns of the related hybrids do not exhibit additional peaks. The CdS phase was not detected due to too small weight content at the TiO_2/Ti surface.

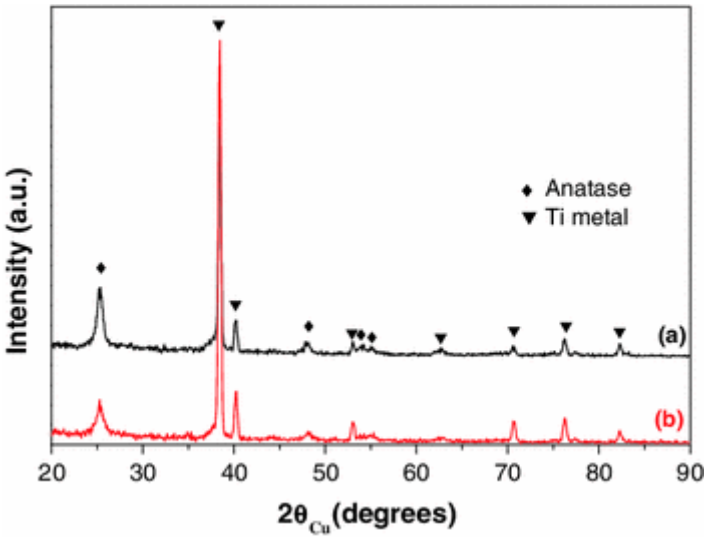

Fig. 4
XRD patterns of **a** TiO_2/Ti and **b** CdS–TiO_2/Ti nanostructures

To confirm that CdS impregnation was successful, XPS analyses of CdS impregnated TiO_2/Ti films were performed. The low-resolution (survey) spectrum presented in Fig. 5exhibits the characteristic peaks of Cd 3d, S 2p, Ti 2p, and O 1s, at about 406, 162, 458, and 530 eV, respectively. The peak calibration is performed with respect to C 1s main peak component of the adventitious carbon set at 285 eV, and includes charge shift correction. High-resolution (HR) spectra of Cd 3d and S 2p are presented in Fig. 6. The Cd 3d core level spectrum (Fig. 6a) exhibits two sharp peaks at 406 ($3d_{5/2}$) and 412 eV ($3d_{3/2}$), in good agreement with the previously reported values for CdS (Xu et al. *1998*; Liu and Chen *2000*; Yang et al. *2007*). The S 2p peak, shown in Fig. 6b, can be fitted with 2 main components, of different intensities; a higher intensity peak at 162.2 eV is attributed to sulfide S^{2-} anion and a lower intensity one at 168.8 eV is attributed to SO_{2-4}, suggesting that the produced CdS QDs are partly oxidized. Such a feature was already observed in the case of TiO_2 nanostructures impregnated with ZnS QDs (Chaguetmi et al. *2013*; Jang et al. *2008*). It was commonly attributed to the reduced size of these nanoparticles and their surface reactivity improvement. High-resolution spectrum of Ti species was also recorded before and after impregnation (not shown). For both samples, two main contributions corresponding to Ti $2p_{3/2}$ and $2p_{1/2}$ were observed at 458.7 and 464.4 eV, respectively, in good agreement with the previously reported XPS data on Ti^{4+}-based oxides (Lu et

al. *2000*; Ohsaki et al. *2001*). There is no evidence of Ti^0 species, suggesting a total surface oxidation during the hydrothermal treatment of Ti sheets.

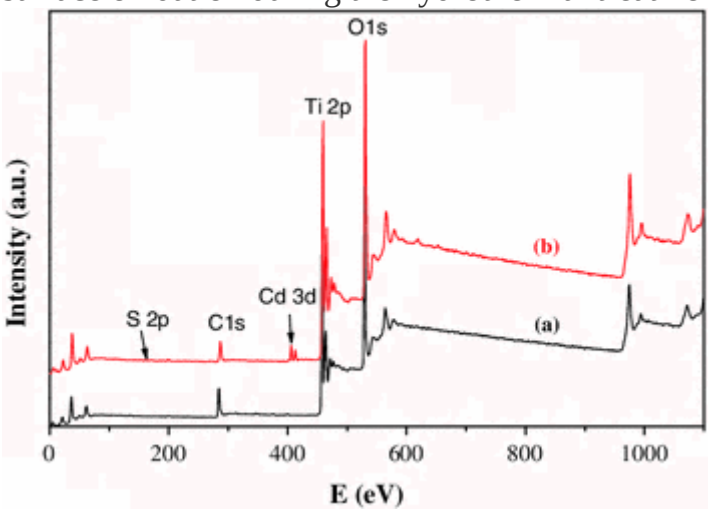

Fig. 5
XPS survey spectra of bare TiO_2/Ti (**a**) and CdS–TiO_2/Ti films (**b**)

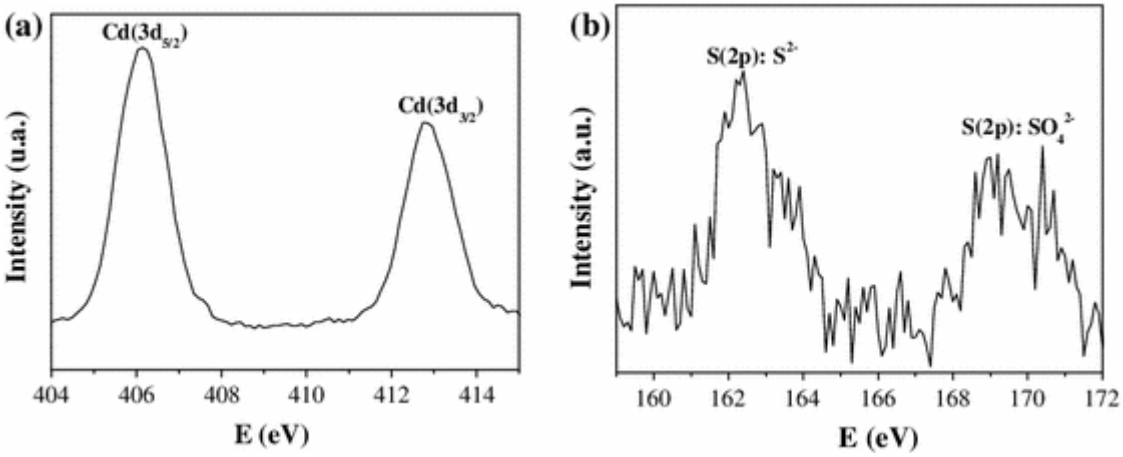

Fig. 6
HR-XPS spectra of Cd 3d (**a**) and S 2p (**b**) for the impregnated CdS–TiO_2/Ti films

The microstructure of the produced CdS–TiO_2/Ti photocatalyst was observed by FEG-SEM and compared to that of bare TiO_2/Ti materials (Fig. 7). Before impregnation, TiO_2 appeared to be constituted by NFs with a diameter of 10–50 nm (Fig. 7a) at the surface of Ti sheets. The NFs stuck and interweaved, with many ramifications, just like a plant root. A hierarchical porous structure exhibiting macropores and mesopores on the Ti plate surface can be thus evidenced (see insets in Fig. 7). After impregnation, TiO_2 NFs appeared less smooth, suggesting a partial coverage by the pre-formed CdS QDs. It was not easy to identify CdS nanocrystals at the surface of the fibers, their very small size escaping from the FEG-SEM imaging resolution. However, the pores present in bare films appeared to be quite filled in the related nanocomposites, suggesting that QDs infiltrated the TiO_2 microstructure (Fig. 7b), forming more or less dense, random multiple nanoparticle layers as previously observed in almost similar materials (Chaguetmi et al. *2013*; Fujii et al. *2001*; Cao et al. *2012*).

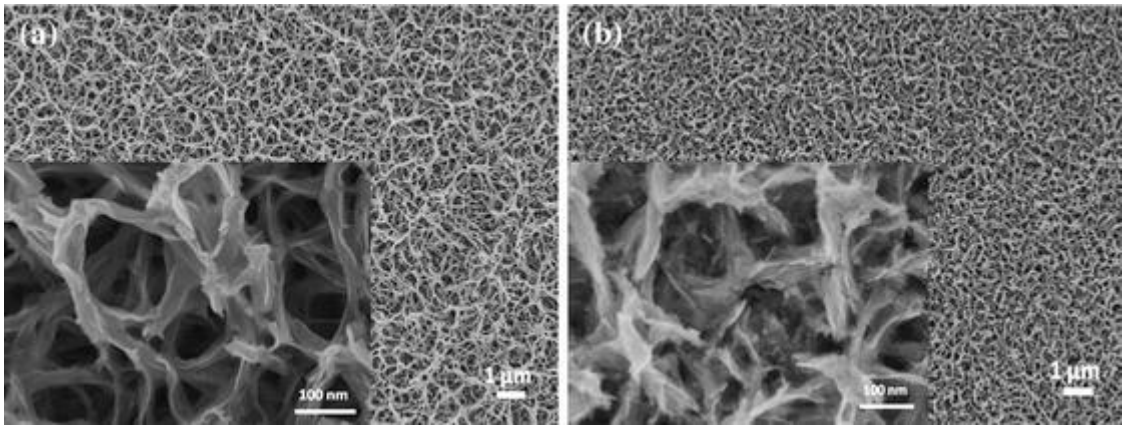

Fig. 7
FEG-SEM image of (**a**) pristine TiO_2/Ti film compared to (**b**) that of its related CdS–TiO_2/Ti nanocomposite. A zoom on the TiO_2 NFs is given on the *inset* for both samples

To have a more precise idea on the CdS covering quality, TEM and HRTEM images were recorded on isolated TiO_2 NFs, peeled from the Ti sheet surface before (Fig. 8a, c) and after CdS impregnation (Fig. 8b, d). The pictures clearly demonstrated good adhesion between CdS QDs and TiO_2 NFs. QDs (surrounded by white circles) were found to be non-aggregated, offering thus the best morphology for the desired application. The QDs coverage, more visible here, appeared to be relatively weak.

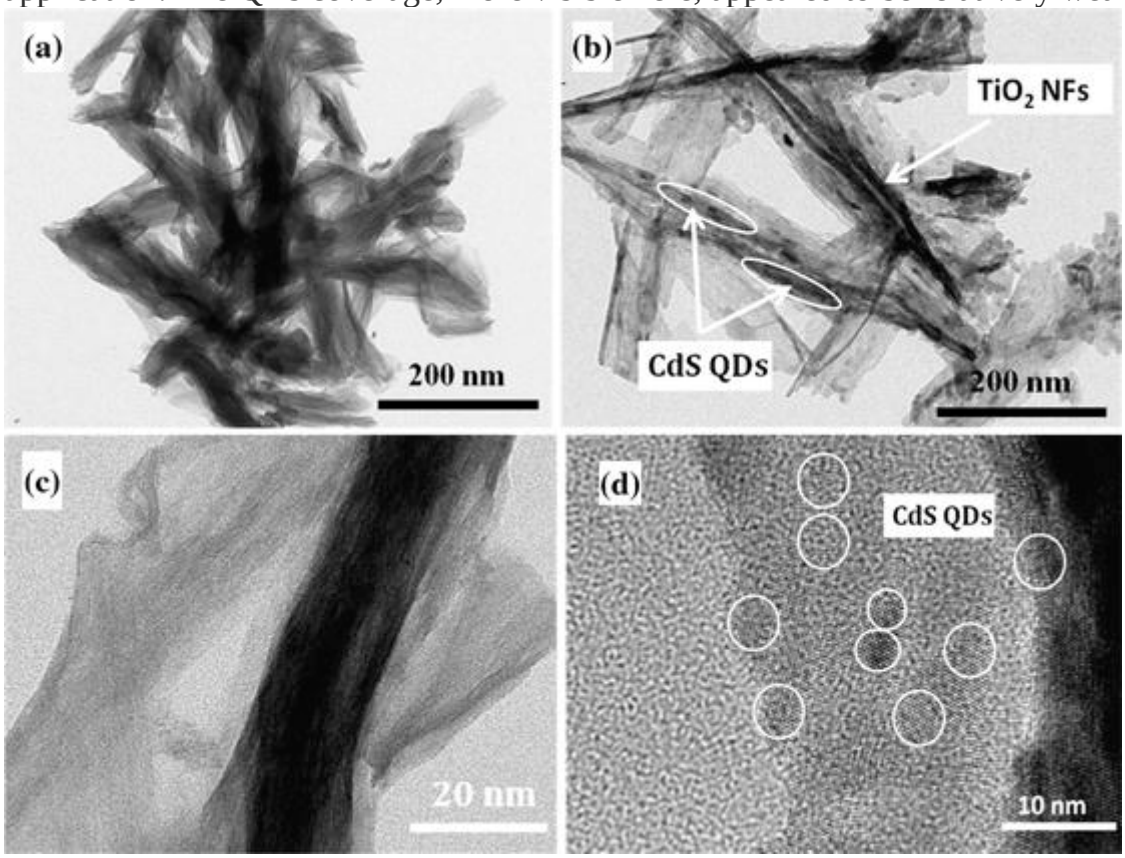

Fig. 8
HRTEM images of representative TiO_2 fibers before (**a**, **c**) and after CdS impregnation (**b**, **d**)

Then, the UV–Vis diffuse reflectance spectra were recorded to compare the absorbance of the prepared CdS–TiO_2/Ti nanocomposites (Fig. 9) to that of pristine

TiO_2/Ti. Few differences could be noticed between the two curves, revealing a similar bandgap between TiO_2/Ti and CdS–TiO_2/Ti materials and confirming the very low amount of QDs adsorbed in the porosity of TiO_2.

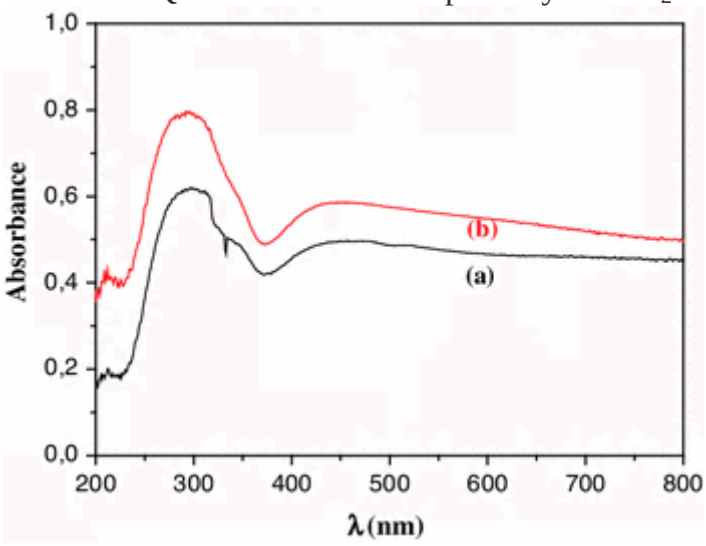

Fig. 9
Absorbance spectra of TiO_2/Ti (**a**) and CdS–TiO_2/Ti nanostructures (**b**)

From these physico-chemical characterization results, we can conclude that QDs should contribute to avoid electron–hole recombination and to improve the photoelectrochemical (PEC) properties of TiO_2/Ti sample; indeed, they were introduced as ultra-diluted species since too many QDs would promote electron–hole recombination and lower charge transfer. Simultaneously, an attentive observation of the recorded spectra indicated that TiO_2 NFs absorbed not only in the UV range, as wide-gap semiconductors, but also in the visible range which is quite surprising. This visible absorption is doubtless due to structural defects in the anatase lattice related to the NFs synthesis conditions. QDs should thus contribute to avoid photogenerated charges trapping by these defects too, making their presence crucial for the desired application.

Photoelectrochemical properties of CdS–TiO_2/Ti nanocomposite films

Photoelectrochemical properties of TiO_2/Ti and CdS–TiO_2/Ti films were evaluated, using a homemade PEC cell. Both photoanodes were illuminated intermittently at a given potential (0 V) for several cycles, to appreciate the reproducibility of their photoresponses (Fig. 10) as well as the stability of the device toward oxidation. Both photoanodes led to an instantaneous change in current upon illumination. The current retracted to the original values almost instantaneously once the illumination is switched off. Several cycles were performed for each sample, for a potential of 0 V bias versus SCE.

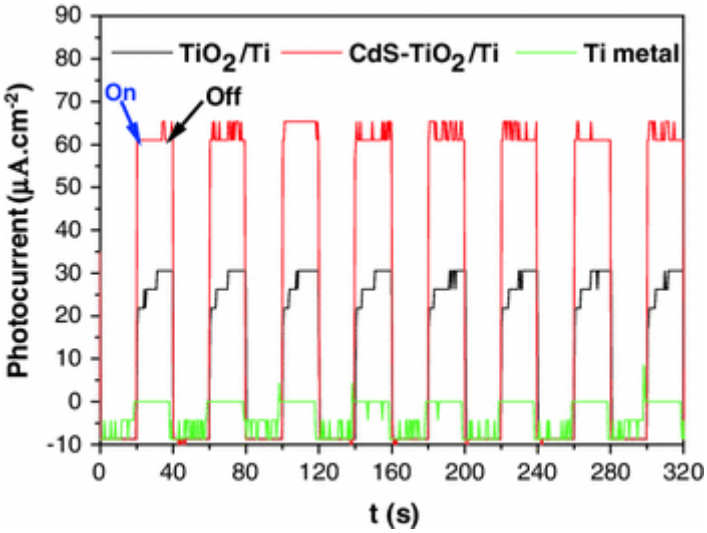

Fig. 10
Photocurrent responses in Na_2SO_4 aqueous solution (0.5 M, pH = 7) of CdS–TiO_2/Ti compared to those of TiO_2/Ti and Ti electrodes under simulated sunlight at 0 V during 320 s

CdS QDs appeared to be particularly valuable to sensitize TiO_2 support, enhancing significantly the photoelectrochemical properties of CdS–TiO_2/Ti compared to those of bare TiO_2/Ti: the photocurrent density produced by CdS–TiO_2/Ti film electrode reached 65 µA cm^{-2}, about twice higher than that measured on TiO_2/Ti film. This improvement has to be underlined, even if this photocurrent value can be considered as relatively weak, probably due to inappropriate back contact resistance. Indeed, one contact to the photoanode was made on the back side of the Ti sheet without removing the thin oxide film that may be built up during hydrothermal processing; this should considerably increase the series resistance. The purity of Ti sheets could be easily improved, in the future, by protecting the back side from corrosion by a stick, which can be removed post-treatment.

Cyclic voltammetry was then performed both in the dark and under simulated solar light to characterize the ability of the samples for PEC cells, through the measurement of J–E curves (Fig. 11). All electrodes led to negligible current under dark conditions. Under illumination, TiO_2/Ti exhibited a great enhancement of the current density after CdS sensitization; a shift in onset potential of about 0.4 V was also observed, suggesting a shift in Fermi level to more negative potential as a result of the coupling between TiO_2 and CdS.

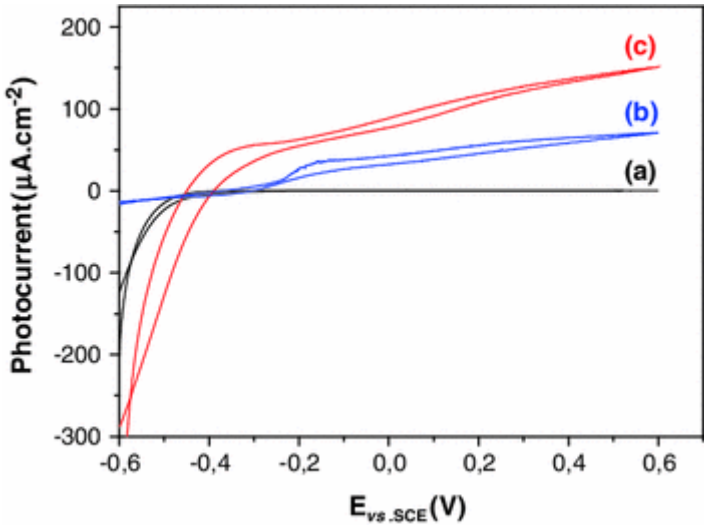

Fig. 11
Photocurrent versus potential curves plotted in the dark for CdS–TiO_2/Ti (**a**) and under simulated sunlight for TiO_2/Ti (**b**) and CdS–TiO_2/Ti (**c**) nanostructures. The potential scan rate was fixed to 10 mV s^{-1}

Electron–hole pairs could be generated by the absorption of photons in both TiO_2nanofibers and CdS QDs if the energies of incident photons are larger than the bandgap; hence, the charge separation is going to be faster than the recombination due the electric field of the depletion regions. The excited electrons are moving through the bulk region to the counter electrode where water reduction occurs while the generated holes are moving toward the electrode/electrolyte interface where water oxidation takes place.

The process of electron injection starts with the absorption by CdS of a photon in the visible region to generate an electron–hole pair (exciton) (Fig. 12). When QDs are irradiated under UV–Vis light source, photogenerated electrons transit from the nanocrystalline QDs valence band (VB) to their conduction band (CB) (Eq. 1). If we consider the energy level diagrams of CdS and TiO_2, the conduction band (CB) of CdS is higher than that of TiO_2. Then, as TiO_2 exhibit a higher dielectric constant, the excited electron is immediately transferred from the CB of CdS to the CB of TiO_2(Eq. 2). Moreover, the enhancement in photocurrent of the CdS-sensitized TiO_2structures is due to the visible light absorption of the CdS QDs since their bandgap is smaller than that of TiO_2. The photogenerated electrons are ultimately transferred to Pt electrode (Eq. 3) through the external circuit. They are subsequently scavenged by hydrogen ion on Pt cathode, forming hydrogen gas (Eq. 4). While, vacant photogenerated holes can contribute to oxygen production at the anode according to the previous results (Cao et al. *2012*; Fujii et al. *2001*; Wu et al. *2012*):

$$CdS-TiO_2+h\upsilon \rightarrow CdS(h^+,e^-)-TiO_2 \quad (1)$$

$$CdS(h^+,e^-)-TiO_2 \rightarrow CdS(h^+)-TiO_2(e^-) \quad (2)$$

$$TiO_2(e^-) \rightarrow Pt(e^-)+TiO_2 \quad (3)$$

$$Pt(e^-)+H^+ \rightarrow Pt+H_2$$

(4)

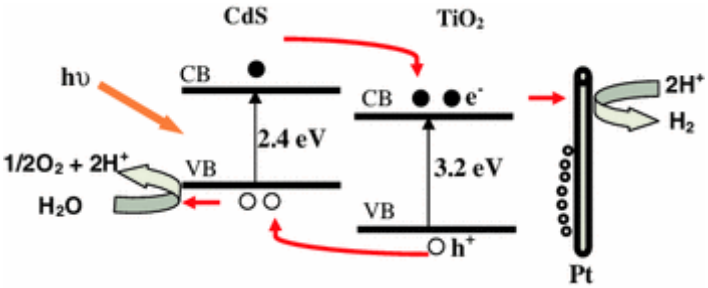

Fig. 12
Schematic representation of TiO_2 possible sensitization mechanism by CdS QDs for hydrogen generation

The measured photoelectrochemical activity of the designed nanocomposite films is directly correlated to hydrogen generation. We are currently building an appropriate cell that allows hydrogen quantification by coupling our homemade PEC cells to a gas chromatography equipment. This part of the work is in progress.

Conclusion

In summary, we described the synthesis of CdS–TiO_2 nanocomposite films via a three-step method which allows to improve our PEC device performance of the components in the final architecture of the desired photoanode before their assembling in an almost easy-to-achieve process, namely impregnation. It involved the production of a thin film of TiO_2 nanofibers (NFs) using a controlled corrosion route of polished Ti sheets and their subsequent direct impregnation by a largely diluted polyol-made CdS quantum dots (QDs) solution.
The photoelectrochemical (PEC) properties of the resulting nanostructures were measured, using a homemade electrochemical cell. A net enhancement of the photocurrent was observed after CdS sensitization, which was found to be twice higher than that of bare TiO_2 NFs in the whole UV–Vis light range. This enhanced PEC, attributed to the increase of the electron–hole separation by the help of the CdS–TiO_2hetero-junction, is promising for efficient photocatalytic applications and hydrogen generation using the solar energy.

References

Allam NK, Grimes CA (2009) Room temperature one-step polyol synthesis of anatase TiO_2 nanotube arrays: photoelectrochemical properties. Langmuir 25:7234–7240. URL..

Asahi R, Morikawa T, Ohwaki T, Aoki K, Taga Y (2001) Visible-light photocatalysis in nitrogen-doped titanium oxides. Science 293(5528):269–271

Bak T, Nowotny J, Rekas M, Sorrell CC (2002) Photoelectrochemical hydrogen generation from water using solar energy: materials-related aspects. Int J Hydrogen Energy 27:991–1022. URL.

Baker DR, Kamat PV (2009) Photosensitization of TiO_2 nanostructures with CdS quantum dots: particulate versus tubular support architectures. Adv Funct Mater 19:805–811. URL.

Banerjee S, Mohapatra SK, Das PP, Misra M (2008) Synthesis of coupled semiconductor by filling 1D TiO_2 nanotubes with CdS. Chem Mater 20:6784–6791. URL.

Cao C, Hu C, Shen W, Wang S, Tian Y, Wang X (2012) Synthesis and characterization of TiO_2/CdS core–shell nanorod arrays and their photoelectrochemical property. J Alloys Compd 523:139–145. URL.

Chaguetmi S, Mammeri F, Nowak S, Decorse P, Lecoq H, Gaceur M, Ben Naceur J, Achour S, Chtourou R, Ammar S (2013) Photocatalytic activity of TiO_2 nanofibers sensitized with ZnS quantum dots. RSC Adv 3:2572–2581. URL.

Chen SG, Paulose M, Ruan C, Mor GK, Varghese OK, Kouzoudis D, Grimes CA (2006) Electrochemically synthesized CdS nanoparticle-modified TiO_2 nanotube-array photoelectrodes: preparation, characterization, and application to photoelectrochemical cells. J Photochem Photobiol A 177:177–184. URL.

Feldman C, Metzmacher C (2001) Polyol mediated synthesis of nanoscale MS particles (M = Zn, Cd, Hg). J Mater Chem 11:2603–2606. URL.

Fujii H, Inata K, Ohtaki M, Eguchi K, Arai H (2001) Synthesis of TiO_2/CdS nanocomposite via TiO_2 coating on CdS nanoparticles by compartmentalized hydrolysis of Ti alkoxide. J Mater Sci 36:527–532. URL.

Gaceur M, Giraud M, Hemadi M, Nowak S, David K, Quisefit JP, Menguy N, Boissière M, Ammar S (2012) Polyol-synthesized $Zn_{0.9}Mn_{0.1}S$ nanoparticles as potential luminescent and magnetic bimodal imaging probes: synthesis, characterization, and toxicity study. J Nanopart Res 14:932–940. URL.

Gao XF, Li HB, Sun WT, Chen Q, Tang FQ, Peng LM (2009) CdTe quantum dots-sensitized TiO_2 nanotube array photoelectrodes. J Phys Chem C 113:7531–7535. URL.

Hensel J, Wang G, Li Y, Jin Y, Zhang Z (2010) Synergistic effect of CdSe quantum dot sensitization and nitrogen doping of TiO_2 nanostructures for photoelectrochemical solar hydrogen generation. Nano Lett 10:478–483. URL.

Jang JS, Kim HG, Joshi UA, Jang JW, Lee JS (2008) Fabrication of CdS nanowires decorated with TiO_2 nanoparticles for photocatalytic hydrogen production under visible light irradiation. Int J Hydrogen Energy 33:5975–5980. URL.

John SE, Mohapatra SK, Misra M (2009) Double-wall anodic titania nanotube arrays for water photooxidation. Langmuir 25:8240–8247. URL.

Kasuga T, Hiramatsu M, Hoson A, Sekino T, Niihara K (1999) Titania nanotubes prepared by chemical processing. Adv Mater 11:1307–1311. URL.

Kawahara T, Konishi Y, Tada H, Tohge N, Nishii J, Ito S (2002) A patterned TiO_2(anatase)/TiO_2(rutile) bilayer-type photocatalyst: effect of the anatase/rutile junction on the photocatalytic activity. Angew Chem Int Ed 41:2811–2813. URL.

Lewis NS, Nocera DG (2006) Powering the planet: chemical challenges in solar energy utilization. Proc Natl Acad Sci USA 103:15729–15735. URL.

Liji-Sobhana SS, Vimala Devi M, Sastry TP, Baran Mandal Asit (2011) CdS quantum dots for measurement of the size-dependent optical properties of thiol capping. J Nanopart Res 13:1747–1757. URL.

Lin CJ, Lu YT, Hsieh CH, Chien SH (2009) Surface modification of highly ordered TiO_2 nanotube arrays for efficient photoelectrocatalytic water splitting. Appl Phys Lett 94:113102.1–113102.3

Liu W, Chen S (2000) An investigation of the tribological behaviour of surface-modified ZnS nanoparticles in liquid paraffin. Wear 238:120–124. URL.

Louie AY (2010) Multimodality imaging probes: design and challenges. Chem Rev 110:3146–3195. URL.

Lu G, Bernasek SL, Schwartz J (2000) Oxidation of a polycrystalline titanium surface by oxygen and water. Surf Sci 458:80–84. URL.

Mor GK, Shankar K, Paulose M, Varghese OK, Grimes CA (2005) Enhanced photocleavage of water using titania nanotube-arrays. Nano Lett 5:191–195. URL.

Ohsaki H, Tachibana Y, Mitsui A, Kamiyama T, Hayashi Y (2001) High rate deposition of TiO_2 by DC sputtering of the TiO_{2-x} target. Thin Solid Films 392:169–175. URL.

Pokhrel S, Huo LH, Zhao H, Gao S (2008) Triangular network of crystalline submicron rutile TiO_2 block assembly: an alcohol sensor. Sens Actuators B 129:18–23. URL.

Seabold JA, Shankar K, Wilke RHT, Paulose M, Varghese OK, Grimes CA, Choi KS (2008) Photoelectrochemical properties of heterojunction CdTe/TiO_2 electrodes constructed using highly ordered TiO_2 nanotube arrays. Chem Mater 20:5266–5273. URL.

Shen Q, Sato T, Hashimoto M, Chen C, Toyoda T (2006) Photoacoustic and photoelectrochemical characterization of CdSe-sensitized TiO_2electrodes composed of nanotubes and nanowires. Thin Solid Films 499:299–305. URL.

Sun WT, Yu Y, Pan HY, Gao XF, Chen Q, Peng LM (2008) CdS quantum dots sensitized TiO_2 nanotube-array photoelectrodes. J Am Chem Soc 130:1124–1125. URL.

Tian YS, Hu CG, He XS, Cao CL, Huang GS, Zhang KY (2010) Titania nanotube arrays for light sensor and UV photometer. Sens Actuators B 144:203–207. URL.

Vogel R, Hoyer P, Weller H (1994) Quantum-sized PbS, CdS, Ag_2S, Sb_2S_3, and Bi_2S_3 particles as sensitizers for various nanoporous wide-bandgap semiconductors. J Phys Chem 98:3183–3188. URL.

Wang CL, Lan S, Xie KP, Lin CJ (2009) Controllable incorporation of CdS nanoparticles into TiO_2 nanotubes for highly enhancing the photocatalytic response to visible light. Sci China Ser B 52:2148–2155. URL.

Wu Y, Long M, Cai W, Dai S, Chen C, Wu D, Bai J (2009) Preparation of photocatalytic anatase nanowire films by in situ oxidation of titanium plate. Nanotechnology 20:185703–185711. URL.

Wu G, Tian M, Chen A (2012) Synthesis of CdS quantum-dot sensitized TiO_2 nanowires with high photocatalytic activity for water splitting. J Photochem Photobiol A 233:65–71. URL.

Xie YB (2006) Photoelectrochemical application of nanotubular titania photoanode. Electrochim Acta 51:3399–3406. URL.

Xu JF, Ji W, Lin JY, Tang SH, Du YW (1998) Preparation of ZnS nanoparticles by ultrasonic radiation method. Appl Phys A 66:639–641. URL.

Yang G, Ma H, Wu Z, Zhang P (2007) Tribological behavior of ZnS-filled polyelectrolyte multilayers. Wear 262:471–476. URL.

Yin YX, Jin ZG, Hou F (2007) Enhanced solar water splitting efficiency using core/sheath heterostructure CdS/TiO_2 nanotube arrays. Nanotechnology 18:495608–495611. URL.

Zhang XW, Lei LC, Zhang JL, Chen QX, Bao JG, Fang B (2009) A novel $CdS/S–TiO_2$ nanotubes photocatalyst with high visible light activity. Sep Purif Technol 66:417–421. URL.

Zhang J, Tang C, Bang JH (2010) $CdS/TiO_2–SrTiO_3$ heterostructure nanotube arrays for improved solar energy conversion efficiency. Electrochem Commun 12:1124–1128. URL..